


 Cite this: *RSC Adv.*, 2020, **10**, 25325

## Enhancement of $\text{CeO}_2$ modified commercial SCR catalyst for synergistic mercury removal from coal combustion flue gas

 Shibo Zhang,<sup>a</sup> Qingzhu Zhang,  <sup>\*a</sup> Yongchun Zhao,  <sup>b</sup> Jianping Yang,<sup>c</sup> Yang Xu<sup>a</sup> and Junying Zhang<sup>\*b</sup>

$\text{CeO}_2$  modified commercial SCR (selective catalytic reduction) catalysts with different  $\text{CeO}_2$  content were prepared and researched for synergistic mercury removal from coal combustion flue gas in this study. The characterization analyses on the catalysts indicated that the introduction of  $\text{CeO}_2$  increased the surface area, the dispersity of the metal oxides on the  $\text{TiO}_2$  support and the redox behavior of the catalyst, which was beneficial to the catalytic activity. The experimental results confirmed that the  $\text{CeO}_2$  loading improved the catalytic efficiencies over the commercial SCR catalyst. The catalyst with a  $\text{CeO}_2$  content of 4% displayed the optimal performance for NO and synergistic  $\text{Hg}^0$  removal, of which the NO conversion and  $\text{Hg}^0$  removal efficiency reached 90.5% and 78.2%, respectively, at 300 °C in simulated coal-fired flue gas. The  $\text{Hg}^0$  removal activity, the independence of  $\text{Hg}^0$  removal from HCl concentration and the effects of  $\text{SO}_2$ , NO and  $\text{NH}_3$  on  $\text{Hg}^0$  removal efficiency all became positive over the modified catalyst compared to over the raw one, which was mainly due to the sufficient chemisorbed oxygen derived from the synergy of  $\text{V}_2\text{O}_5$  and  $\text{CeO}_2$  and the redox transformation between  $\text{Ce}^{3+}$  and  $\text{Ce}^{4+}$  on the catalyst surface. The  $\text{CeO}_2$  modification generated a significant enhancement on the catalytic performance and made the commercial SCR catalyst more suitable to be employed for NO and synergistic mercury removal in a coal combustion power plant.

Received 15th May 2020

Accepted 28th June 2020

DOI: 10.1039/d0ra04350h

[rsc.li/rsc-advances](http://rsc.li/rsc-advances)

## 1. Introduction

Mercury is a kind of extremely harmful pollutant in the ecological environment. It poses a serious threat to human health due to its hypertoxicity, persistence and bio-accumulation.<sup>1</sup> According to the Global Mercury Assessment 2018 issued by the UN Environment Programme, the global anthropogenic mercury emission reached 2150 tons in 2015, which increased by 12% compared to that in 2010.<sup>2</sup> Significant coal burning is one of the main reasons for the growth of mercury emissions. And coal combustion power plants are considered as the major anthropogenic source of mercury release.<sup>3</sup> As the Minamata Convention on Mercury came into force in August 2017, the limit on mercury emission from coal-fired power plants will be more rigorous on the basis of the existing regulations.<sup>4</sup> Therefore, it is urgent to pay extensive attention to mercury emission control of coal combustion

power plants under the dual pressure of environmental protection and convention fulfillment.

Mercury in coal-fired flue gas exists mainly in the types of elemental  $\text{Hg}$  ( $\text{Hg}^0$ ), oxidized  $\text{Hg}$  ( $\text{Hg}^{2+}$ ) and particle bound  $\text{Hg}$  ( $\text{Hg}^P$ ).  $\text{Hg}^{2+}$  and  $\text{Hg}^P$  can be respectively captured by wet flue gas desulfurization (WFGD) and particulate matter control device (PMCD) of power plant because of their physical properties, while  $\text{Hg}^0$  is difficult to be controlled by the single pollutant control equipment due to its volatility and water insolubility.<sup>5,6</sup> So the key to the control of mercury emission from coal combustion power plant is the removal of  $\text{Hg}^0$ . Similarly with mercury,  $\text{NO}_x$  is also a sort of hazardous contaminant with great harm to environment that coal burning releases, and NO occupies about 95% among  $\text{NO}_x$ .<sup>7-9</sup> Currently, the method of selective catalytic reduction (SCR) is generally used by coal-fired power plants for NO removal. Besides, the SCR catalyst has the capacity of oxidizing  $\text{Hg}^0$  to  $\text{Hg}^{2+}$  due to the existence of active oxygen on its surface, followed by  $\text{Hg}^{2+}$  being removed in the downstream WFGD.<sup>10,11</sup> Compared with other  $\text{Hg}$  removal plans such as sorbent injection, utilizing SCR catalyst to synergistically remove  $\text{Hg}$  is remarkably cost-effective and meanwhile beneficial to the avoiding of secondary mercury pollution.<sup>12</sup> Hence, it is promising for coal-fired power plant to adopt this approach to deal with the  $\text{Hg}$  removal from flue gas. And the

<sup>a</sup>Environment Research Institute, Shandong University, Qingdao 266237, China.  
 E-mail: zqz@sdu.edu.cn

<sup>b</sup>State Key Laboratory of Coal Combustion, School of Energy and Power Engineering, Huazhong University of Science and Technology, Wuhan 430074, China. E-mail: jyzhang@hust.edu.cn

<sup>c</sup>School of Energy Science and Engineering, Central South University, Changsha 410083, China



research on the synergistic  $Hg^0$  oxidation with SCR catalyst has attracted more attention in recent years.

The commercial SCR catalyst that is currently used by coal combustion power plants is the  $TiO_2$ -supported  $V_2O_5$ - $WO_3$ / $TiO_2$  catalyst. A series of studies have been made on the  $Hg^0$  oxidation over the  $V_2O_5$ - $WO_3$ / $TiO_2$  catalyst. The results indicated that the  $V=O$  bond on the catalyst surface could participate in  $Hg^0$  oxidation as the active sites. The  $Hg^0$  removal efficiency over the catalyst could reach 60–80% in general, and sometimes the efficiency was even higher than 90%.<sup>13,14</sup> The increases of  $V_2O_5$  loading, surface area and reaction temperature are in favor of the  $Hg^0$  oxidation activity.<sup>15</sup> Especially, the existence of HCl in the flue gas had an obvious promotion on the  $Hg^0$  oxidation over the  $V_2O_5$ -based catalysts.  $Hg^0$  removal efficiency of  $V_2O_5$ - $WO_3$ / $TiO_2$  was close to 100% at 380 °C with 4.5 mmol m<sup>-3</sup> HCl contained in the reaction gas.<sup>16</sup> The  $SiO_2$ - $TiO_2$ - $V_2O_5$  catalyst likewise showed a  $Hg^0$  removal efficiency of nearly 100% in the co-presence of  $O_2$  and HCl.<sup>17</sup> And the facilitation of HCl on the efficiency of commercial SCR catalyst was also testified by kinetic analysis.<sup>18</sup> However, though the commercial  $V_2O_5$ - $WO_3$ / $TiO_2$  catalyst displays certain  $Hg^0$  removal capacity under the appropriate conditions, it has apparent drawbacks such as the narrow working temperature range and the limited  $Hg^0$  removal efficiency at the SCR operating temperature.<sup>16,19</sup> Meanwhile, the effectiveness of  $Hg^0$  removal depends heavily on the HCl concentration. The efficiency could be as high as 90% in the flue gas derived from burning high-rank coal, while in flue gas of burning low-rank coal only less than 30% was observed.<sup>17,20,21</sup> This condition is distinctly disadvantageous to those power plants that combust sub-bituminous coal or lignite. So it is necessary to make modification on commercial SCR catalyst to improve its catalytic properties. In recent years,  $CeO_2$ -based catalysts have gradually come into view of researchers due to its prominent catalytic activity. Related studies demonstrated that element Ce would help enhance the oxygen storage capacity of the catalyst, which led to the superior performance on NO and  $Hg^0$  removal. Illustratively, Gao *et al.*<sup>22</sup> prepared  $CeO_2$ / $TiO_2$  catalyst by sol-gel method and found the NO conversion of the catalyst reached 93.4–98.6% in the wide temperature range of 250–450 °C; Li *et al.*<sup>23</sup> investigated  $Hg^0$  removal activity of  $CeO_2$ / $TiO_2$  in simulated coal-fired flue gas and confirmed the optimal efficiency could attain 94%, and efficient  $Hg^0$  oxidation could be achieved even in the absence of HCl; Fan *et al.*<sup>24</sup> acquired that the zeolite supported  $CeO_2$ /HZSM-5 catalyst exhibited  $Hg^0$  removal efficiency of more than 95% among the range of 120–320 °C; Wang *et al.*<sup>25</sup> loaded  $CeO_2$  on Ti-based pillared interlayered clays to examine the simultaneous NO and  $Hg^0$  removal efficiency over the catalyst, and the results showed that the NO conversion was almost 100% at 350 °C while  $Hg^0$  removal efficiency also reached higher than 50% in the same condition. In view of the advantage of the activity of catalyst containing  $CeO_2$ , it is reasonable to speculate that using  $CeO_2$  to modify the  $V_2O_5$ - $WO_3$ / $TiO_2$  catalyst will make a significant improvement on the catalytic properties of the catalyst. Zhao *et al.*<sup>19</sup> has previously modified the  $TiO_2$  support with  $CeO_2$  and synthesized  $V_2O_5$ - $WO_3$ / $TiO_2$ - $CeO_2$  catalyst, and the experimental study confirmed the enhancement of  $Hg^0$  removal performance of the catalyst,

such as the efficiency and sulfur-resistance, resulted from the addition of  $CeO_2$ . Some literatures also prepared the  $CeO_2$  modified  $V_2O_5$ - $WO_3$ ( $MoO_3$ )/ $TiO_2$  to investigate the NO removal activity specifically, and the satisfactory NO conversions, sulfur-resistance and alkali metal resistance were obtained over the catalysts.<sup>26–28</sup> Nevertheless, few literatures have made investigations on the effectiveness of employing  $CeO_2$  to directly modify the commercial SCR catalyst of power plant for synergistic  $Hg^0$  removal so far, which is of great value and close correlation to practical application. Moreover, the present commercial SCR catalyst is not replaceable in the short term, though some researched novel catalysts such as Mn-based, Cu-based, noble metal and perovskite structure catalysts displayed considerable  $Hg^0$  removal efficiency in the lab-scale tests.<sup>29–32</sup> Thus, it can be seen that it is of great significance to examine the synergistic  $Hg^0$  removal performance of the  $CeO_2$  modified commercial  $V_2O_5$ - $WO_3$ / $TiO_2$  catalyst.

Based on the above presentations, this work takes  $CeO_2$  modified commercial SCR catalyst as the researching object, and conducts the experiments in simulated coal combustion flue gas (SFG). NO removal performance of the catalysts with different  $CeO_2$  loadings were first tested considering the primary purpose of SCR. Then the  $Hg^0$  removal activity of the catalysts was investigated in detail.  $Hg^0$  removal efficiencies over different  $CeO_2$ -loading catalysts at different temperatures were evaluated, and the effects of individual flue gas components in SFG on the efficiency were detected as well. The characterization analyses of X-ray fluorescence (XRF), Brunauer–Emmett–Teller (BET), X-ray diffraction (XRD),  $H_2$ -Temperature Programmed Reduction ( $H_2$ -TPR) and X-ray photoelectron spectroscopy (XPS) were carried out to understand physical-chemical properties of the catalysts and explore the modification mechanism of  $CeO_2$ . The study results of this work will present application prospect of the  $CeO_2$  modification on commercial SCR catalyst for improving the catalytic performance.

## 2. Materials and methods

### 2.1. Catalyst preparation

The honeycomb commercial SCR catalyst employed in this study was got from a catalyst corporation of China which professionally produces SCR catalyst of coal-fired power plant. The  $CeO_2$  modified catalysts were prepared by the solution impregnation method. The honeycomb catalyst was grinded to powder first and sieved with a 200 mesh sifter. Then a certain amount of the sieved fine catalyst powder was placed in a beaker, followed by the  $Ce(NO_3)_3$  aqueous solution which contained the desired quantity of  $Ce(NO_3)_3$  being filled into the beaker. The obtained slurry was stirred for 1 h and then exposed to an ultrasonic bath for 2 h. After the mixture was dried at 110 °C for 12 h and calcinated in air at 500 °C for 4 h sequentially, the final  $CeO_2$  modified commercial SCR catalyst was acquired. The mass fractions of  $CeO_2$  of 1%, 2%, 4% and 7% in the modified catalysts were designed. In the process of preparing the catalysts with different  $CeO_2$  loadings, the weight of the original catalyst powder was remained unchanged, and



the  $\text{CeO}_2$  loading was controlled by the solvent amount of the added  $\text{Ce}(\text{NO}_3)_3$  aqueous solution. The  $\text{CeO}_2$  modified catalysts were abbreviated as (x) $\text{CeO}_2$ -SCR (x represents the mass fraction of  $\text{CeO}_2$ ) in the later sections, and the catalyst without modification was designated as raw SCR. Additionally, the pure  $\text{CeO}_2$  catalyst was also prepared for comparison, which used  $\text{Ce}(\text{NO}_3)_3$  as the precursor as well to maintain the consistency.

## 2.2. Catalyst characterizations

The characterization methods of XRF, BET, XRD,  $\text{H}_2$ -TPR and XPS were carried out over the fresh and spent catalyst samples in order to understand the physical and chemical properties of the catalysts and analyze the  $\text{CeO}_2$  modification mechanism. The XRF analysis was conducted with an EAGLE III focusing fluorescence spectrograph which was operated at 38 kV. The measurement of the BET surface was accomplished on an ASAP 2020 porosimeter by means of  $\text{N}_2$  adsorption. The XRD analysis was performed using an X'Pert PRO diffractometer ( $\text{Cu K}\alpha$  radiation) of which the working voltage and emission current were 40 kV and 40 mA, respectively, with the scanning angle ranging from  $10^\circ$  to  $80^\circ$  ( $\theta$ ). The test of  $\text{H}_2$ -TPR was carried out on an Autochem 2920 analyzer with the operating temperature raised from  $30^\circ\text{C}$  to  $850^\circ\text{C}$  at a rate of  $10^\circ\text{C min}^{-1}$ , and the reaction gas was  $50\text{ mL min}^{-1}$  10%  $\text{H}_2$ /Ar. The XPS technique was implemented on a PerkinElmer PHI 5100 ESCA system with  $\text{Al K}\alpha$  X-ray source ( $h\nu = 1486.6\text{ eV}$ ) to study the valence states of the elements and using the C 1s binding energy value of 284.6 eV for the spectra calibration.

## 2.3. Catalytic activity measurement

The experimental system used in this work was similar to that employed in our previous studies,<sup>33–35</sup> as described in Fig. 1. Briefly, the flue gas components ( $\text{N}_2$ ,  $\text{O}_2$ ,  $\text{HCl}$ ,  $\text{SO}_2$ ,  $\text{NO}$ , and  $\text{NH}_3$ ) came from standard cylinder gases and their gas flow was accurately controlled by the corresponding calibrated mass flowmeter, respectively. Water vapor ( $\text{H}_2\text{O}$ ) was produced by a steam generator. The continuous feed of  $\text{Hg}^0$  vapor of approximately  $60\text{ }\mu\text{g m}^{-3}$  was generated from a  $\text{Hg}^0$  penetration tube (VICI, Metronics Inc., Santa Clara, CA) which was placed in a U-tube and heated by a water bath, with  $\text{N}_2$  carrying the  $\text{Hg}^0$

vapor into the flue gas. The catalytic reaction was made to occur in a fixed bed reactor with a temperature controller to set the reaction temperature. The  $\text{NO}$  and  $\text{Hg}^0$  concentrations in the flue gas were measured by a gas analyzer (AFRISO, Multilyzer STe, M60) and a  $\text{Hg}^0$  online monitor (Ohio Lumex, RA-915M), respectively. And the  $\text{N}_2\text{O}$  and  $\text{NO}_2$  concentrations were monitored with a FTIR analyzer (Gasmet Dx4000). Several specific gas-washing bottles were added for eliminating the acid gas to prevent corrosion and interferences on the monitoring devices. The gas line of the system was heated by electric heating belt to avoid any possible adsorption of the gas components on the line before the measurement. The exhaust gas was purified by active carbon before discharged to atmosphere.

The experiments of this work were carried out under the condition of simulated coal-fired flue gas of which the composition was 4%  $\text{O}_2$ , 10 ppm  $\text{HCl}$ , 800 ppm  $\text{SO}_2$ , 400 ppm  $\text{NO}$ , 400 ppm  $\text{NH}_3$ , 8%  $\text{H}_2\text{O}$  and  $60\text{ }\mu\text{g m}^{-3}$   $\text{Hg}^0$  with  $\text{N}_2$  to balance unless otherwise noted. The total flow of the flue gas was controlled at  $1\text{ L min}^{-1}$ . The catalyst dosage was 0.5 g for each test, and the space velocity (GHSV) was correspondingly about  $50\,000\text{ h}^{-1}$ . In each test, the flue gas was first introduced to the bypass, and the concentrations of  $\text{NO}$  and  $\text{Hg}^0$  at the inlet of the reactor were acquired when the readings of the monitoring devices reached stability. Then the gas stream was switched to pass through the catalyst until the stable  $\text{NO}$  and  $\text{Hg}^0$  concentrations at the outlet of the reactor were obtained as well. The stability was defined as the fluctuation of the concentrations being no more than 5% for a period of at least 30 min. After each step of the experiment, the spent catalyst was replaced by fresh sample before starting the next test. The  $\text{NO}$  conversion,  $\text{N}_2$  selectivity and  $\text{Hg}^0$  removal efficiency adopted to evaluate the catalytic activity of the catalyst were respectively calculated by eqn (1)–(3) as follows.

$$\text{NO conversion (\%)} = \frac{\text{NO}_{\text{in}} - \text{NO}_{\text{out}}}{\text{NO}_{\text{in}}} \times 100\% \quad (1)$$

$$\begin{aligned} \text{N}_2 \text{ selectivity (\%)} = & \frac{\text{NO}_{\text{in}} - \text{NO}_{\text{out}} - 2 \times \text{N}_2\text{O}_{\text{out}} - \text{NO}_2_{\text{out}}}{\text{NO}_{\text{in}} - \text{NO}_{\text{out}}} \\ & \times 100\% \end{aligned} \quad (2)$$

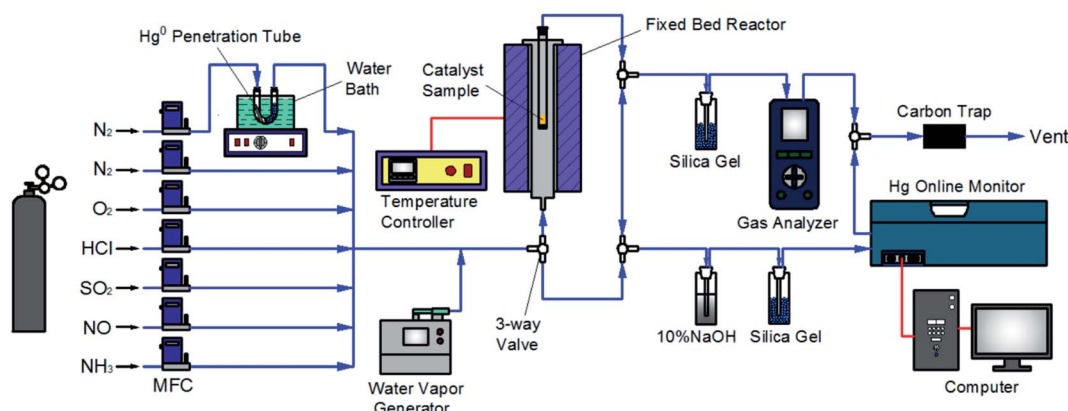


Fig. 1 Schematic diagram of the experimental system.



$$\text{Hg}^0 \text{ removal efficiency (\%)} = \frac{\text{Hg}_{\text{in}}^0 - \text{Hg}_{\text{out}}^0}{\text{Hg}_{\text{in}}^0} \times 100\% \quad (3)$$

The subscript “in” and “out” in the equations represented the gas concentrations at the inlet and outlet of the reactor, respectively. As the outlet  $\text{Hg}^0$  concentration was read when it achieved a stable value, the catalyst was in the state of  $\text{Hg}$  saturated adsorption at this time and all the removed  $\text{Hg}$  was gaseous  $\text{Hg}^{2+}$ . Additionally, the researched catalysts were verified to have almost no capacity for  $\text{Hg}^0$  removal at room temperature. So the physical adsorption of  $\text{Hg}^0$  was negligible, and the defined  $\text{Hg}^0$  removal efficiency here was equal to  $\text{Hg}^0$  oxidation efficiency.

### 3. Results and discussion

#### 3.1. Characterization of the $\text{CeO}_2$ -SCR catalysts

**3.1.1 XRF analysis.** XRF analysis was adopted to investigate the element compositions and contents of the catalysts. The results were summarized in Table 1. Before the loading of  $\text{CeO}_2$ , the content of  $\text{V}_2\text{O}_5$  which was the active component and the content of  $\text{WO}_3$  using for improving the thermal stability and surface acidity in raw SCR catalyst were 0.98% and 6.63%, respectively. Both the values were among the ranges of the contents of  $\text{V}_2\text{O}_5$  and  $\text{WO}_3$  in usual honeycomb commercial SCR catalyst, which were respectively 0.5–3% and 2–10%. The activity of SCR catalyst was generally in proportion to the content of  $\text{V}_2\text{O}_5$ . But exorbitant vanadium content would lead to the growing  $\text{SO}_2/\text{SO}_3$  conversion.<sup>36</sup> The  $\text{V}_2\text{O}_5$  content of the raw SCR catalyst employed in this work was a moderate percent of about 1%, indicating this catalyst was well typical and representative. Small amount of  $\text{SiO}_2$  was also detected to contain in the catalyst, which was helpful for boosting the mechanical strength. For the  $\text{CeO}_2$  modified catalysts, the practical contents of  $\text{CeO}_2$  in the catalysts with different  $\text{CeO}_2$  loadings were very close to the corresponding designed values, which testified the accuracy of the preparation of the catalysts. Meanwhile, the addition of  $\text{CeO}_2$  did not cause apparent variations on the contents of  $\text{V}_2\text{O}_5$ ,  $\text{WO}_3$  and  $\text{SiO}_2$  in the catalysts.

**3.1.2 BET analysis.** The surface structural properties of the  $\text{CeO}_2$  modified commercial SCR catalysts tested by BET analysis were listed in Table 2. According to the results, the surface area of the raw catalyst was at a relatively low level of  $18.64 \text{ m}^2 \text{ g}^{-1}$ ,

Table 1 Element compositions and contents of the  $\text{CeO}_2$  modified commercial SCR catalysts

Catalyst	Mass fraction (%)				
	$\text{CeO}_2$	$\text{TiO}_2$	$\text{V}_2\text{O}_5$	$\text{WO}_3$	$\text{SiO}_2$
Raw SCR	0	90.71	0.98	6.63	1.68
1% $\text{CeO}_2$ -SCR	0.92	89.73	0.96	6.58	1.81
2% $\text{CeO}_2$ -SCR	1.95	88.54	1.08	6.80	1.63
4% $\text{CeO}_2$ -SCR	4.03	86.93	1.12	6.35	1.57
7% $\text{CeO}_2$ -SCR	6.79	84.18	1.20	6.06	1.77

Table 2 Surface structural properties of the  $\text{CeO}_2$  modified commercial SCR catalysts

Catalyst	BET surface area ( $\text{m}^2 \text{ g}^{-1}$ )	Pore volume ( $\text{cm}^3 \text{ g}^{-1}$ )	Pore size (nm)
Raw SCR	18.64	0.069	19.579
1% $\text{CeO}_2$ -SCR	69.23	0.287	16.555
2% $\text{CeO}_2$ -SCR	66.39	0.279	17.081
4% $\text{CeO}_2$ -SCR	64.92	0.285	17.248
7% $\text{CeO}_2$ -SCR	61.83	0.233	15.553
Pure $\text{CeO}_2$	66.28	0.294	17.835

which might result from the specific preparation process of the catalyst corporation. The introduction of  $\text{CeO}_2$  made a significant enhancement on the surface area and pore volume of the catalyst. The surface area increased dramatically from  $18.64 \text{ m}^2 \text{ g}^{-1}$  to  $69.23 \text{ m}^2 \text{ g}^{-1}$  with the loading of only 1%  $\text{CeO}_2$ . The increase of surface area could raise the amount of the active sites available for  $\text{Hg}^0$  and other reactants on the catalyst surface, thereby it usually being beneficial to the catalytic activity.<sup>35,37</sup> And the enlargement of pore volume was also in favor of the  $\text{Hg}^0$  removal capacity of the catalyst. The surface area showed a slight declined trend as the  $\text{CeO}_2$  loading augmented, which was probably due to the blockage of some surface micropores caused by the increasing  $\text{CeO}_2$  loading.<sup>38,39</sup> It's worth noting that the surface area of the  $\text{CeO}_2$  modified catalysts was much closer to that of pure  $\text{CeO}_2$  than to the raw SCR catalyst, indicating that the surface area was obviously altered and controlled by  $\text{CeO}_2$  though it occupied only a minor proportion in the catalysts. By contrast, the pore size of the catalyst was not distinctly affected by the addition of  $\text{CeO}_2$ , and the change was small.

**3.1.3 XRD analysis.** The crystalline characteristic in the catalysts was investigated by XRD analysis, and the result was shown in Fig. 2. On the patterns of raw SCR catalyst and pure  $\text{CeO}_2$ , only the peaks corresponding to anatase  $\text{TiO}_2$  and  $\text{CeO}_2$  were discovered respectively.<sup>23,30,40</sup> With  $\text{CeO}_2$  doped into the commercial SCR catalyst, the peak intensity of  $\text{TiO}_2$  became weak gradually, and meanwhile the peak standing for  $\text{CeO}_2$  was not detected when the  $\text{CeO}_2$  content was lower than 4%. This

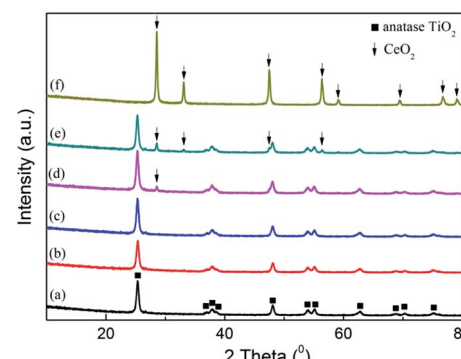


Fig. 2 XRD patterns of the catalysts ((a) raw SCR, (b) 1%  $\text{CeO}_2$ -SCR, (c) 2%  $\text{CeO}_2$ -SCR, (d) 4%  $\text{CeO}_2$ -SCR, (e) 7%  $\text{CeO}_2$ -SCR, (f) pure  $\text{CeO}_2$ ).



phenomenon suggested that there existed some interaction between  $\text{TiO}_2$  and  $\text{CeO}_2$  in the catalysts.<sup>33,41,42</sup>  $\text{CeO}_2$  was well dispersed and in the form of amorphous phase on the catalyst surface. As the  $\text{CeO}_2$  content reached 4%, a peak corresponding to  $\text{CeO}_2$  emerged on the pattern at  $28.6^\circ$ , indicating that the present load amount has made the dispersion of  $\text{CeO}_2$  on the catalyst reach the critical point of saturation. Further increasing the  $\text{CeO}_2$  loading would lead to the conversion of the doped  $\text{CeO}_2$  from amorphous phase to crystalline state. The emergence of distinct characteristic peaks corresponding to  $\text{CeO}_2$  on the profile of 7%  $\text{CeO}_2$ -SCR confirmed this inference. In addition, the peaks of  $\text{V}_2\text{O}_5$  and  $\text{WO}_3$  were not discovered on any catalyst pattern, displaying an amorphous distribution as well. More active substance existed in the amorphous phase was considered to be advantageous for the catalytic activity of the catalyst, while the appearance of the crystal of the active species was adverse to the catalytic performance.<sup>43,44</sup>

### 3.2. NO removal performance of the $\text{CeO}_2$ -SCR catalysts

Considering the primary function of SCR catalyst was to remove NO for coal combustion power plant, NO removal activity of the  $\text{CeO}_2$  modified commercial SCR catalysts in simulated coal-fired flue gas was first examined prior to the investigation on  $\text{Hg}^0$  removal performance. The experimental results were shown in Fig. 3. The NO conversions of the catalysts showed a growing trend as the reaction temperature increased from  $150^\circ\text{C}$  to  $400^\circ\text{C}$ . The optimal temperature range was  $300\text{--}400^\circ\text{C}$  which was consistent with that of literature report.<sup>41,45,46</sup> NO conversion over the raw SCR catalyst in this range was 74.6–84.3%, which was a little lower than the efficiencies monitored in power plants. This might be attributed to the higher GHSV in the lab reactor than that under the practical conditions ( $2000\text{--}3000\text{ h}^{-1}$ ),<sup>47</sup> which led to the shorter contact time between flue gas and catalyst. As  $\text{CeO}_2$  was added into the catalyst, NO conversion was apparently promoted. And the catalyst with the  $\text{CeO}_2$  loading of 4% exhibited the best activity for NO removal. The NO conversions were 90.5%, 92.5% and 89.3%, respectively, at the temperature points of  $300\text{--}400^\circ\text{C}$  over 4%  $\text{CeO}_2$ -SCR. Besides, the efficiency of 4%  $\text{CeO}_2$ -SCR could also reach nearly

80% at  $250^\circ\text{C}$ . Thus, the  $\text{CeO}_2$  modification not only improved NO conversion of commercial SCR catalyst, but also broadened the working temperature and enhanced the medium-low temperature activity of the catalyst. The superior NO removal performance of 4%  $\text{CeO}_2$ -SCR was associated with the higher content of  $\text{CeO}_2$  dispersed in the amorphous phase, while the slightly decreased NO conversion over 7%  $\text{CeO}_2$ -SCR compared to that over 4%  $\text{CeO}_2$ -SCR might be due to the generation of  $\text{CeO}_2$  crystal in the catalyst. Additionally, the surface area was also a possible influence factor for the NO removal activity because the variation trend of the surface area was very close to that of the NO conversion among 4%  $\text{CeO}_2$ -SCR, 7%  $\text{CeO}_2$ -SCR and the raw catalyst. Therefore, the experimental acquirement was in good agreement with the characterization results. The efficiency of pure  $\text{CeO}_2$  was in a poor level among the testing temperature range, indicating that the element V was still responsible for the nice NO removal activity of  $\text{CeO}_2$ -SCR though  $\text{CeO}_2$  generated modification effects on the catalysts. To sum up, the  $\text{CeO}_2$  modification led to an advancement upon the property of the commercial SCR catalyst and made it own prominent NO removal activity, which established a solid foundation on the utilization of the catalyst for synergistic  $\text{Hg}^0$  removal.

As another important evaluation index for NO removal performance,  $\text{N}_2$  selectivity was measured over the 4%  $\text{CeO}_2$ -SCR catalyst which exhibited the highest NO conversion, and the results were shown in Fig. 4. Under SFG, the  $\text{N}_2$  selectivity over the catalyst reduced slightly with the increase of the reaction temperature, which was caused by the generation of a small amount of  $\text{N}_2\text{O}$  and  $\text{NO}_2$  during the reaction. The detected concentrations of  $\text{N}_2\text{O}$  were much higher than those of  $\text{NO}_2$ . So the decrease of the  $\text{N}_2$  selectivity was mainly due to the  $\text{N}_2\text{O}$  generation at the higher temperatures. Nevertheless, the  $\text{N}_2\text{O}$  generation was lower than 15 ppm in the whole temperature range of  $150\text{--}400^\circ\text{C}$ , and even the poorest  $\text{N}_2$  selectivity measured at  $400^\circ\text{C}$  reached as high as 90.5%. Hence, the catalyst displayed great  $\text{N}_2$  selectivity in the NO removal process, further confirming the excellent NO removal performance of the  $\text{CeO}_2$ -SCR catalyst in the simulated coal-fired flue gas.

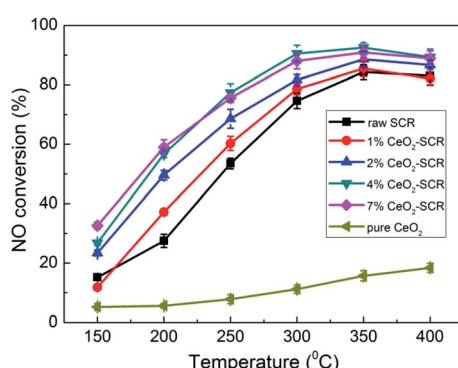


Fig. 3 NO conversion over the  $\text{CeO}_2$  modified commercial SCR catalysts under different reaction temperatures in simulated coal-fired flue gas.

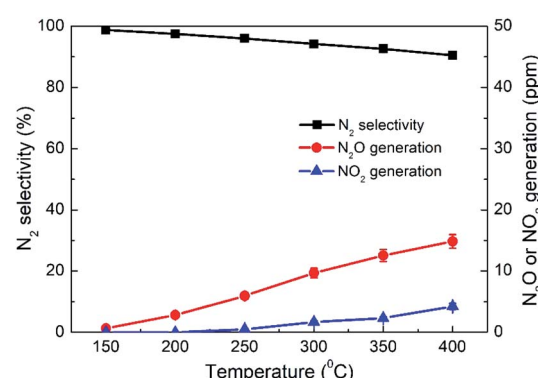


Fig. 4  $\text{N}_2$  selectivity and  $\text{N}_2\text{O}$  and  $\text{NO}_2$  generations over 4%  $\text{CeO}_2$ -SCR under different reaction temperatures in simulated coal-fired flue gas.



### 3.3. $\text{Hg}^0$ removal performance of the $\text{CeO}_2$ -SCR catalysts

**3.3.1  $\text{Hg}^0$  removal efficiency under different temperatures in SFG.**  $\text{Hg}^0$  removal performance of the  $\text{CeO}_2$  modified commercial SCR catalysts was then investigated as the emphasis. First, the  $\text{Hg}^0$  removal efficiencies of the catalysts in simulated coal-fired flue gas were measured under different reaction temperatures, and the results were shown in Fig. 5. As the temperature increased, the variation trend of the  $\text{Hg}^0$  removal efficiencies of the  $\text{CeO}_2$ -SCR catalysts was opposite to that of the NO conversions, and it was a descending tendency. The possible reason for this phenomenon was that the lower temperature was beneficial to the  $\text{Hg}^0$  adsorption on the catalyst which was an essential procedure for  $\text{Hg}^0$  removal, and the  $\text{Hg}^0$  oxidation was realized mainly through the form of adsorbed  $\text{Hg}^0$  ( $\text{Hg}_{\text{ad}}$ ).<sup>35,42,48</sup> The introduction of  $\text{CeO}_2$  into the catalyst accelerated the  $\text{Hg}^0$  removal efficiency apparently. Analogously to the testing results of NO removal activity, the optimal sample for  $\text{Hg}^0$  removal was 4%  $\text{CeO}_2$ -SCR as well, which corresponded to the characterization results again.  $\text{Hg}^0$  removal efficiency of 4%  $\text{CeO}_2$ -SCR achieved more than 90% in the temperature range of 150–250 °C. Even at 300 °C which was among the conventional operating temperature of SCR catalyst (300–400 °C), 4%  $\text{CeO}_2$ -SCR also exhibited the efficiency of as high as 78.2% on the basis of NO conversion guaranteed at 89.3%. So the catalyst showed remarkable activity for simultaneous NO and  $\text{Hg}^0$  removal. The prominent performance for synergistic  $\text{Hg}^0$  removal was mainly owed to the sufficient chemisorbed oxygen ( $\text{O}_{\text{ad}}$ ) of 4%  $\text{CeO}_2$ -SCR led by the existence of  $\text{Ce}^{3+}/\text{Ce}^{4+}$  ion pair and the oxygen transfer between them in the catalyst,<sup>38,49</sup> which would be confirmed by the subsequent XPS analysis. The abundant  $\text{O}_{\text{ad}}$  would facilitate  $\text{Hg}^0$  oxidation to generate  $\text{HgO}$  as the active species. The related reaction process was described by eqn (4)–(6). As the efficiencies of the raw catalyst and pure  $\text{CeO}_2$  were no more than 38.3%, the superior performance of the  $\text{CeO}_2$  modified commercial SCR catalyst was also primarily resulted from the synergy of  $\text{V}_2\text{O}_5$  and  $\text{CeO}_2$  in the catalyst.<sup>50</sup> In addition, considering the GHSV was much higher in the experimental condition than in actual flue gas of power plant, the catalytic efficiencies might be preferable in practical

application. Hence, the SCR catalyst manifested to be more competent and promising for commercial use after the  $\text{CeO}_2$  modification.



### 3.3.2 Effects of the flue gas components on $\text{Hg}^0$ removal efficiency

Effect of each flue gas component on the  $\text{Hg}^0$  removal efficiency of the  $\text{CeO}_2$ -SCR catalyst was then investigated to reveal its role in  $\text{Hg}^0$  removal process. And the results were made comparison with those of the raw SCR catalyst to explore the reasons for the modification effect of  $\text{CeO}_2$  on the catalyst for  $\text{Hg}^0$  removal in simulated coal-fired flue gas. Because the optimum catalytic efficiencies were implemented at 300 °C over 4%  $\text{CeO}_2$ -SCR with the NO conversion and synergistic  $\text{Hg}^0$  removal efficiency being 89.3% and 78.2%, respectively, the experiments of this part were carried out at 300 °C using 4%  $\text{CeO}_2$ -SCR as the catalyst sample. The reaction atmosphere was SFG with the concentration of the investigated component changed and the others constant.

**3.3.2.1. Effect of HCl.** As the important oxidant for  $\text{Hg}^0$  oxidation in coal combustion flue gas, effect of HCl on the  $\text{Hg}^0$  removal efficiency of the catalysts was examined, and the results were shown in Fig. 6. For the raw catalyst,  $\text{Hg}^0$  removal efficiency was disadvantaged in the absence of HCl, and the highest value was only 27%. Even though 10 ppm HCl was added into the flue gas, the efficiency was still maintained at a low level since it was below 40% in the whole temperature range. Only when the HCl concentration increased from 10 ppm to 30 ppm did the  $\text{Hg}^0$  removal efficiency of the raw catalyst show a significant improvement. It increased by 35.5% and 45.4%, respectively, at 250 °C and 300 °C as the instances. The above results verified the viewpoint in the literatures that the commercial SCR catalyst was qualified to be utilized in the flue gas derived from burning bitumite with high HCl content while not appropriate to work under low HCl concentration caused by

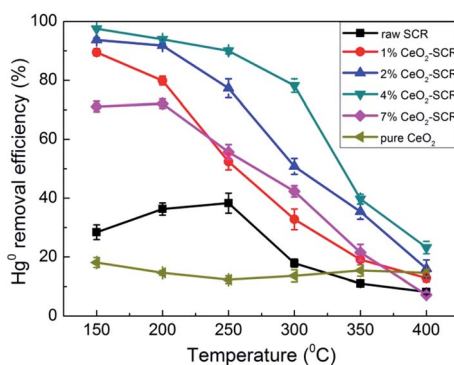


Fig. 5  $\text{Hg}^0$  removal efficiency over the  $\text{CeO}_2$  modified commercial SCR catalysts under different reaction temperatures in simulated coal-fired flue gas.

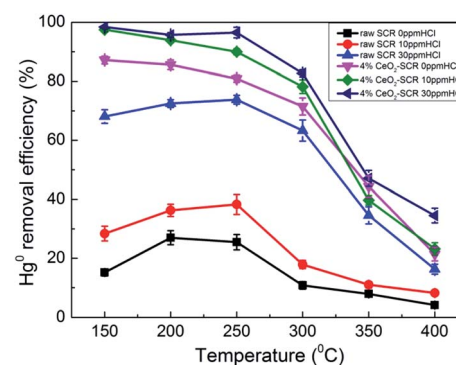


Fig. 6 Effect of HCl on  $\text{Hg}^0$  removal efficiency of raw SCR catalyst and 4%  $\text{CeO}_2$ -SCR in simulated coal-fired flue gas (reaction gas: SFG with 0, 10, 30 ppm HCl).



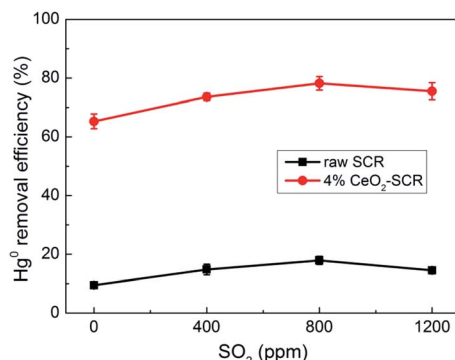


Fig. 7 Effect of SO<sub>2</sub> on Hg<sup>0</sup> removal efficiency of raw SCR catalyst and 4% CeO<sub>2</sub>-SCR in simulated coal-fired flue gas (reaction gas: SFG with 0, 400, 800, 1200 ppm SO<sub>2</sub>).

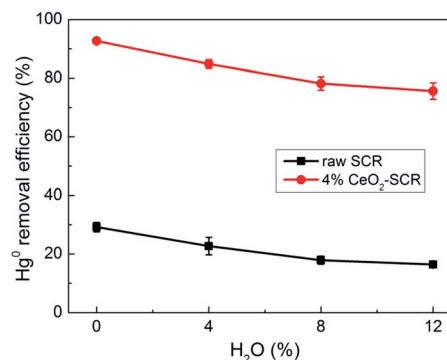
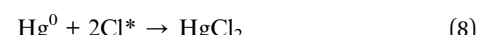


Fig. 9 Effect of H<sub>2</sub>O on Hg<sup>0</sup> removal efficiency of raw SCR catalyst and 4% CeO<sub>2</sub>-SCR in simulated coal-fired flue gas (reaction gas: SFG with 0, 4, 8, 12% H<sub>2</sub>O).

using low-rank coals for Hg<sup>0</sup> removal.<sup>20,23</sup> By contrast, after CeO<sub>2</sub> modification, 4% CeO<sub>2</sub>-SCR exhibited much more prominent Hg<sup>0</sup> removal efficiency than raw SCR catalyst under the same HCl concentration. The performance over 4% CeO<sub>2</sub>-SCR was even better without HCl than that over the raw catalyst in the presence of 30 ppm HCl. A limited increase of the efficiency of 4% CeO<sub>2</sub>-SCR was observed as the HCl concentration raised. Nevertheless, the catalyst displayed satisfactory Hg<sup>0</sup> removal activity when exposed to 10 ppm HCl. The Hg<sup>0</sup> removal efficiencies were excellent at 150–300 °C. Therefore, the CeO<sub>2</sub> modification weakened the dependence of Hg<sup>0</sup> removal activity of the catalyst on HCl content of the flue gas. This was really good news for power plants combusting sub-bituminous coal and lignite which occupied the majority of all items. The reason for the superior Hg<sup>0</sup> removal efficiency of 4% CeO<sub>2</sub>-SCR under low HCl concentration was also due to the improved content of O<sub>ad</sub> on the catalyst surface. More HCl could be converted by the abundant O<sub>ad</sub> to form active Cl (Cl<sup>\*</sup>) which had strong oxidation, followed by Hg<sup>0</sup> being oxidized to HgCl<sub>2</sub> by Cl<sup>\*</sup>.<sup>51,52</sup> Through this way, the introduced CeO<sub>2</sub> enhanced the HCl utilization of the catalyst. The involved reactions could be

described by eqn (7) and (8). Meanwhile, this was also one of the main reasons for the higher Hg<sup>0</sup> removal efficiency over 4% CeO<sub>2</sub>-SCR compared to that over raw SCR in the simulated coal-fired flue gas besides the direct oxidation by O<sub>ad</sub>.



**3.3.2.2. Effect of SO<sub>2</sub>.** Effect of SO<sub>2</sub> on the Hg<sup>0</sup> removal efficiency was shown in Fig. 7. The variation trends of Hg<sup>0</sup> removal efficiency of raw SCR catalyst and 4% CeO<sub>2</sub>-SCR were almost the same with the rising SO<sub>2</sub> concentration. The efficiency was promoted first as the SO<sub>2</sub> content in the flue gas increased from 0 to 800 ppm. The promotion could be explained by SO<sub>3</sub> generated from SO<sub>2</sub> oxidation, and then Hg<sup>0</sup> reacted with SO<sub>3</sub> to form HgSO<sub>4</sub>,<sup>10</sup> as described by eqn (9) and (10). The increase range of the efficiency was a little larger over 4% CeO<sub>2</sub>-SCR than over raw catalyst, which was probably because the adequate O<sub>ad</sub> in 4% CeO<sub>2</sub>-SCR converted more SO<sub>2</sub> to SO<sub>3</sub> that had the ability

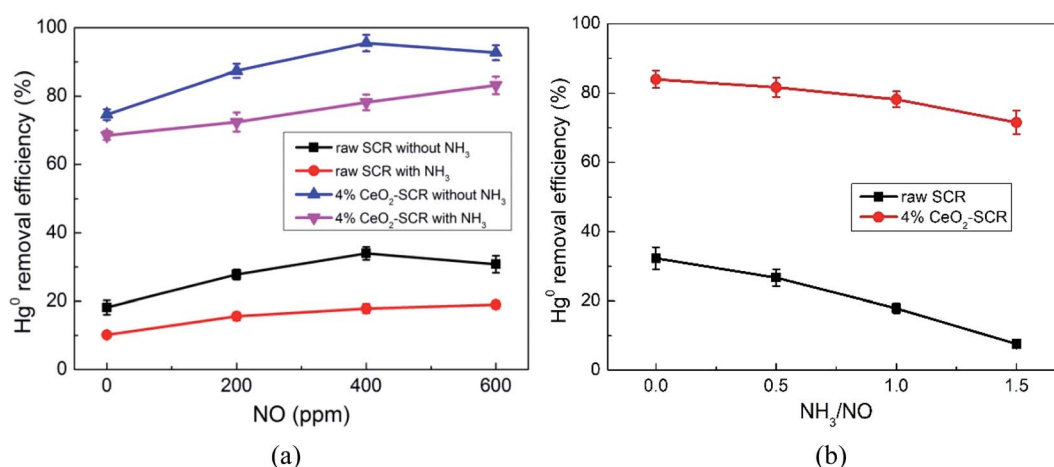


Fig. 8 Effects of NO and NH<sub>3</sub> on Hg<sup>0</sup> removal efficiency of raw SCR catalyst and 4% CeO<sub>2</sub>-SCR in simulated coal-fired flue gas ((a) effect of NO, reaction gas: SFG with 0, 200, 400, 600 ppm NO in the presence or absence of NH<sub>3</sub>; (b) effect of NH<sub>3</sub>, reaction gas: SFG with 0, 200, 400, 600 ppm NH<sub>3</sub>).



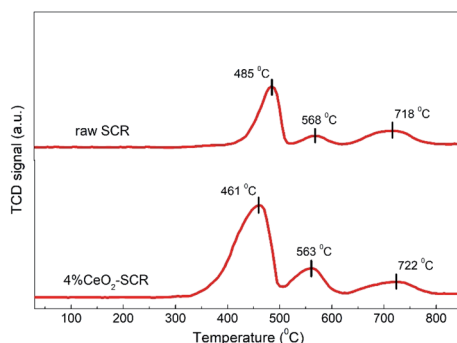


Fig. 10  $\text{H}_2$ -TPR profiles of the raw SCR and 4%  $\text{CeO}_2$ -SCR catalysts.

to oxidize  $\text{Hg}^0$  and facilitated the proceeding of eqn (10). As  $\text{SO}_2$  content further increased to 1200 ppm, the efficiency suffered slight inhibition, which might be due to the generation of vanadium sulfate and/or cerium sulfate under the high  $\text{SO}_2$  concentration that caused the deactivation of the catalyst to some extent.<sup>53,54</sup> Compared to the dramatic decrease of the  $\text{Hg}^0$  removal efficiency over Mn-based catalysts in the presence of  $\text{SO}_2$ ,<sup>34,55</sup> the commercial V-based catalyst exhibited the advantage of owning excellent sulfur-resistance distinctly.



**3.3.2.3. Effects of NO and  $\text{NH}_3$ .** NO and  $\text{NH}_3$  were the principal reactants of the SCR de $\text{NO}_x$  reaction. Effects of NO and

$\text{NH}_3$  in the flue gas on  $\text{Hg}^0$  removal efficiency were important factors for determining the performance of a catalyst for synergistic  $\text{Hg}^0$  removal. The testing results on raw SCR and 4%  $\text{CeO}_2$ -SCR were shown in Fig. 8. The increase of NO concentration without the injection of  $\text{NH}_3$  generated the influence of promoting first and then restraining on the efficiencies of both the catalysts, as shown in Fig. 8(a). NO could be oxidized by chemisorbed oxygen on the catalyst to  $\text{NO}_2$  which had the capacity to oxidize  $\text{Hg}^0$  to  $\text{Hg}(\text{NO}_3)_2$ .<sup>47</sup> The related reactions were presented by eqn (11) and (12). And it was the reason for the improvement of the  $\text{Hg}^0$  removal efficiency with the raise of NO concentration. As the NO content further increased after it has reached 400 ppm, the excessive NO would lead to the generation of materials such as nitrite which had no  $\text{Hg}^0$  oxidation capacity and easily caused pore plugging on the catalyst surface besides  $\text{NO}_2$ ,<sup>56</sup> resulting in the diminishment of the  $\text{Hg}^0$  removal efficiency. Under the condition of  $\text{NH}_3$  added, the proceeding of SCR de $\text{NO}_x$  reaction removed NO in the flue gas, and the actual concentration of NO was shrunken. Thus, it showed a gradual increase trend of the efficiency as NO content lifted from 0 to 600 ppm, and the inhibition was not formed. Similarly to the effect of  $\text{SO}_2$ , the promotion of NO on the efficiency of 4%  $\text{CeO}_2$ -SCR was more evident than on the efficiency of raw catalyst, which was owed to the more sufficient  $\text{O}_{\text{ad}}$  in 4%  $\text{CeO}_2$ -SCR accelerating the proceeding of eqn (11) and (12) as well. The existence of  $\text{NH}_3$  suppressed  $\text{Hg}^0$  removal efficiency apparently. This judgment could be viewed more intuitively from the results in Fig. 8(b). The increase of the ratio of  $\text{NH}_3/\text{NO}$  in the flue gas led to obvious inhibitive effect on the efficiencies over both the raw and modified catalysts.  $\text{NH}_3$  was considered to form intense competitive adsorption with  $\text{Hg}^0$  on the surface, hindering the

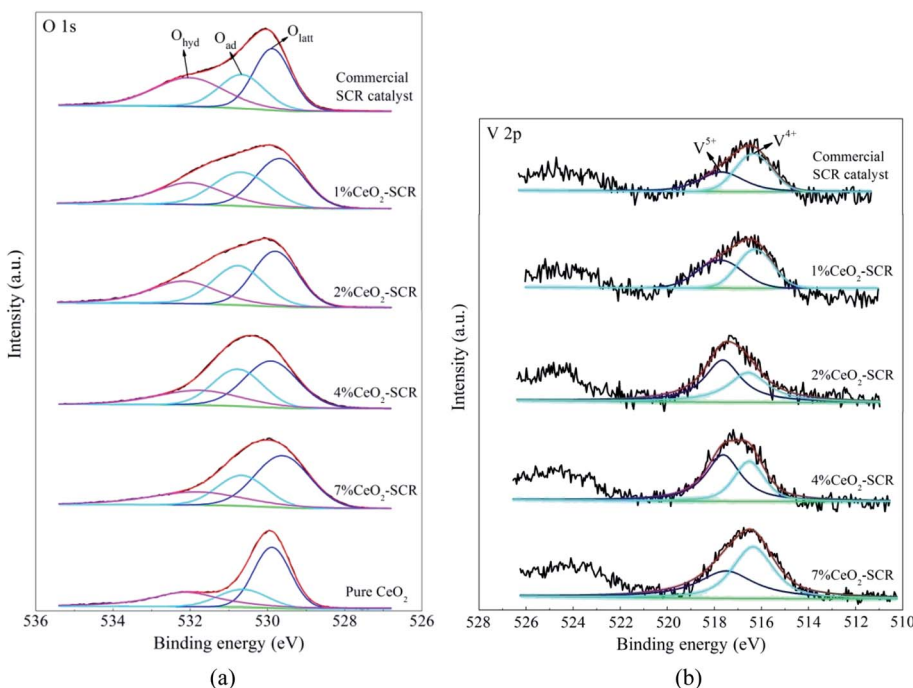


Fig. 11 XPS spectra of O 1s and V 2p for the fresh raw and  $\text{CeO}_2$  modified commercial SCR catalysts ((a) O 1s; (b) V 2p).



necessary  $\text{Hg}^0$  adsorption process and also the following  $\text{Hg}^0$  oxidation.<sup>42,57,58</sup> It was worth noting that the inhibition of  $\text{NH}_3$  on the  $\text{Hg}^0$  removal efficiency was weaker over 4%  $\text{CeO}_2$ -SCR than over the raw catalyst. The reasonable explanation was that the modified catalyst owned stronger NO removal activity. More  $\text{NH}_3$  was expended in NO removal reaction so that the inhibition on  $\text{Hg}^0$  removal was weakened. In this view, the  $\text{CeO}_2$  modification made the catalyst display better  $\text{NH}_3$ -resistance in  $\text{Hg}^0$  removal process, and the property of the catalyst for synergistic  $\text{Hg}^0$  removal was thereby reinforced.



**3.3.2.4. Effect of  $\text{H}_2\text{O}$ .** A certain amount of water vapor ( $\text{H}_2\text{O}$ ) was contained in coal-fired flue gas since water was one of the components of coal. Effect of  $\text{H}_2\text{O}$  on the  $\text{Hg}^0$  removal efficiency was investigated, and the results were shown in Fig. 9.  $\text{H}_2\text{O}$  generated an unfavorable influence on the efficiency. It declined by a close extent over the raw catalyst and 4%  $\text{CeO}_2$ -SCR as 8%  $\text{H}_2\text{O}$  was added into the flue gas. The inhibitive

action could be attributed to the competitive adsorption between  $\text{H}_2\text{O}$  and the reactants of  $\text{Hg}^0$  oxidation such as  $\text{Hg}^0$  and  $\text{HCl}$  on the catalyst.<sup>59</sup> As  $\text{H}_2\text{O}$  content was augmented from 8% to 12%, the downward trend of the efficiency was visibly diminished, which was perhaps because the common adsorption sites for  $\text{Hg}^0$ ,  $\text{HCl}$  and  $\text{H}_2\text{O}$  were limited and the further increase of  $\text{H}_2\text{O}$  concentration would not aggravate the inhibition.<sup>34</sup> Based on the results, the inhibition of  $\text{H}_2\text{O}$  on the  $\text{Hg}^0$  removal efficiency was not intense in general.

### 3.4. Modification mechanism of $\text{CeO}_2$ explored by XPS analysis

According to the above experimental results, the  $\text{CeO}_2$  modification generated excellent results on the NO and  $\text{Hg}^0$  removal performance of commercial SCR catalyst. The characterization results of BET and XRD could present the related reasons for the modification effects in a certain degree. In order to further explore the modification mechanism of  $\text{CeO}_2$  on the catalyst,  $\text{H}_2\text{-TPR}$  and XPS analyses were carried out to detect the redox behavior and valence states (or types) of the elements in the raw and modified catalysts.

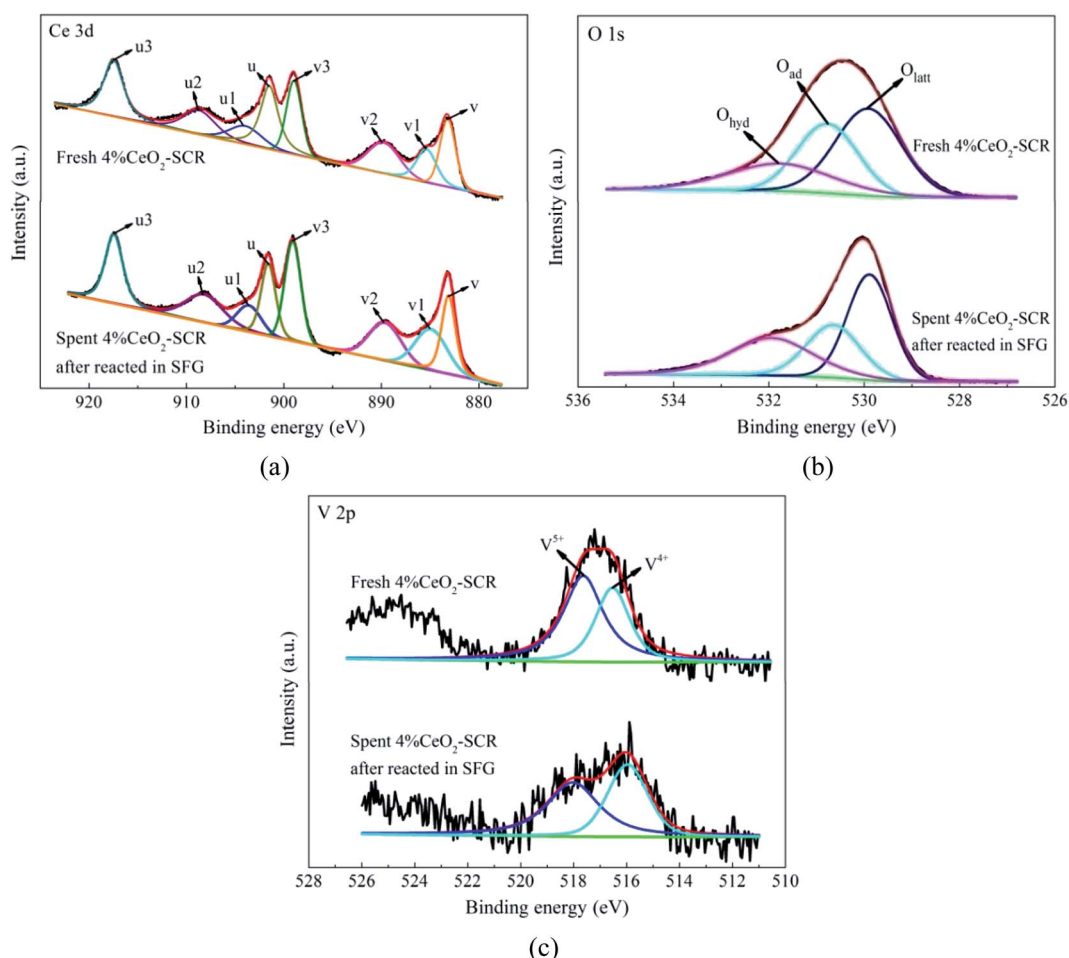


**Fig. 12** XPS spectra of Ce 3d, O 1s and V 2p for the fresh 4%  $\text{CeO}_2$ -SCR catalyst and the spent 4%  $\text{CeO}_2$ -SCR catalyst after reacted in SFG ((a) Ce 3d; (b) O 1s; (c) V 2p).



**Table 3** The surface atomic contents of O and the ratios of  $O_{ad}$  and  $V^{5+}$  in the corresponding elements on the catalysts determined by XPS

Catalyst	Content of O (%)	$O_{ad}/(O_{latt} + O_{ad} + O_{hyd})$ (%)	Content of $O_{ad}$ (%)	$V^{5+}/(V^{4+} + V^{5+})$ (%)
Raw SCR	46.0	26.1	12.0	43.5
1% CeO <sub>2</sub> -SCR	64.9	31.0	20.1	48.0
2% CeO <sub>2</sub> -SCR	64.6	31.4	20.3	56.4
4% CeO <sub>2</sub> -SCR	62.6	32.5	20.4	60.8
7% CeO <sub>2</sub> -SCR	57.4	25.8	14.8	46.1
Pure CeO <sub>2</sub>	46.2	19.8	9.1	—

**3.4.1 H<sub>2</sub>-TPR analysis.** H<sub>2</sub>-TPR analysis was implemented over the raw SCR and 4% CeO<sub>2</sub>-SCR catalysts, and the results were shown in Fig. 10. On the profile of the raw catalyst, the peaks emerged at 485 °C and 568 °C could be attributed to the reduction of  $V^{5+}$  and surface oxygen, respectively, and the broad shoulder peak at around 720 °C was corresponded to the overlap of the reduction of  $W^{6+}$  and lattice oxygen.<sup>44,60,61</sup> By contrast, a reduction peak was observed at 461 °C on the profile of 4% CeO<sub>2</sub>-SCR. As Ce<sup>4+</sup> was reported to reduce at about 470 °C, this peak was considered to be the overlapped reduction peak of  $V^{5+}$  and Ce<sup>4+</sup>.<sup>62</sup> It was evident that the temperature of this peak was lowered and the intensity was strengthened dramatically compared to the peak of the raw catalyst at 485 °C, which indicated that the synergy of element V and Ce reinforced the reactivity of the catalyst. In addition, the reduction peak of surface oxygen of 4% CeO<sub>2</sub>-SCR at 563 °C was much stronger than that of the raw catalyst, so it demonstrated the existence of Ce enhanced the oxygen storage capacity of the catalyst. Combining the above factors, the integral area of the reduction profile was obviously larger over 4% CeO<sub>2</sub>-SCR than over the raw catalyst, suggesting the improved redox behavior of the catalyst led by the CeO<sub>2</sub> modification. The superior redox behavior was favorable to the NO and Hg<sup>0</sup> removal performance, which was one of main reasons for the prominent catalytic efficiencies of the CeO<sub>2</sub> modified commercial SCR catalyst.

**3.4.2 XPS analysis.** The XPS spectra of the elements for the fresh catalysts, together with the fitting results of the curves, were shown in Fig. 11. For the spectra of O 1s, the fitting peaks were assigned to lattice oxygen ( $O_{latt}$ ), chemisorbed oxygen ( $O_{ad}$ ) and oxygen of hydroxyl and free water ( $O_{hyd}$ ) in sequence at the binding energies from small to large,<sup>25,63</sup> as shown in Fig. 11(a). And the fitting peaks of V 2p at the binding energies of approximately 516.4 eV and 517.6 eV could be distributed to  $V^{4+}$  and  $V^{5+}$ , respectively,<sup>64,65</sup> which was shown in Fig. 11(b). In addition, the analysis on the spent catalyst sample of 4% CeO<sub>2</sub>-

SCR after reacted in simulated coal-fired flue gas was conducted as well. The obtained curves of Ce 3d, O 1s and V 2p were made comparisons with those of the fresh catalyst, and the results were shown in Fig. 12. On the curves of the element Ce as shown in Fig. 12(a), the fitting peaks of u, u2, u3, v, v2 and v3 were attributed to Ce<sup>4+</sup>, while the peaks of u1 and v1 were corresponded to Ce<sup>3+</sup>.<sup>38,66</sup> And the spectra of O and V for the spent catalyst were shown respectively in Fig. 12(b) and (c). The ratios of each elemental type or valence state in the corresponding elements of the catalysts were acquired through integrating the fitting peaks and calculating the peak area. The calculation results for the elements of the fresh and spent catalysts were summarized in Tables 3 and 4, respectively.

According to the testing results, the addition of CeO<sub>2</sub> into the catalyst improved both the surface atomic content of O and the proportion of  $O_{ad}$ , which led to the increase of the content of  $O_{ad}$  on the catalyst, as the data listed in Table 3. It could be judged from the results of Ce 3d of 4% CeO<sub>2</sub>-SCR shown in Fig. 12(a) and Table 4 that Ce<sup>3+</sup> and Ce<sup>4+</sup> coexisted in the modified catalysts. The presence of Ce<sup>3+</sup> with a proportion of 16.6% could create charge imbalance and unsaturated chemical bonds on the surface, which was favorable for the generation of chemisorbed oxygen, thereby raising the content of  $O_{ad}$  and boosting the oxygen storage capacity of the catalyst.<sup>38,61,67</sup>  $O_{ad}$  was the active oxygen species that could participate in the catalytic reactions. 4% CeO<sub>2</sub>-SCR owned the highest content of  $O_{ad}$  among the catalysts, which was another important reason for its optimal NO and Hg<sup>0</sup> removal performance. As the CeO<sub>2</sub> loading increased from 4% to 7%, the  $O_{ad}$  content on the catalyst declined and it was even lower than that of the raw catalyst. This result could be associated with the conversion of CeO<sub>2</sub> to the crystalline phase in 7% CeO<sub>2</sub>-SCR according to the XRD results, which made it disadvantaged for the forming of  $O_{ad}$  from the loaded CeO<sub>2</sub>, and meanwhile the forming of crystalline CeO<sub>2</sub> might consume a number of the intrinsic  $O_{ad}$  on the surface. Besides  $O_{ad}$ , the intensity of the  $V^{5+}$  peak and the ratio of  $V^{5+}$  were also enlarged with the introduction of CeO<sub>2</sub>. The increase of the  $V^{5+}$  proportion might be attributed to part of  $V^{4+}$  being oxidized by the abundant  $O_{ad}$  to  $V^{5+}$  on the modified catalysts.  $V^{5+}$  was the active species in V-based catalyst as well, which had good oxidation and was beneficial to Hg<sup>0</sup> removal activity. So the adequate  $O_{ad}$  was also presented in the form of  $V_2O_5$ . As the content of  $O_{ad}$  on the surface of pure CeO<sub>2</sub> did not show an advantage, it further demonstrated the superior oxygen storage capacity was the result of the synergy of CeO<sub>2</sub> and  $V_2O_5$  in the CeO<sub>2</sub>-SCR catalysts.

After the 4% CeO<sub>2</sub>-SCR catalyst was reacted in SFG, the XPS spectra of O 1s and V 2p for the spent catalyst were compared

**Table 4** The ratios of Ce<sup>3+</sup>,  $O_{ad}$  and  $V^{5+}$  in the corresponding elements on the fresh and spent 4% CeO<sub>2</sub>-SCR catalysts determined by XPS

Catalyst	Ce <sup>3+</sup> /(Ce <sup>4+</sup> + Ce <sup>3+</sup> ) (%)	$O_{ad}/(O_{latt} + O_{ad} + O_{hyd})$ (%)	$O_{hyd}/(O_{latt} + O_{ad} + O_{hyd})$ (%)	$V^{5+}/(V^{4+} + V^{5+})$ (%)
Fresh 4% CeO <sub>2</sub> -SCR	16.6	32.5	22.8	60.8
Spent 4% CeO <sub>2</sub> -SCR after reacted in SFG	20.5	27.0	30.2	54.7



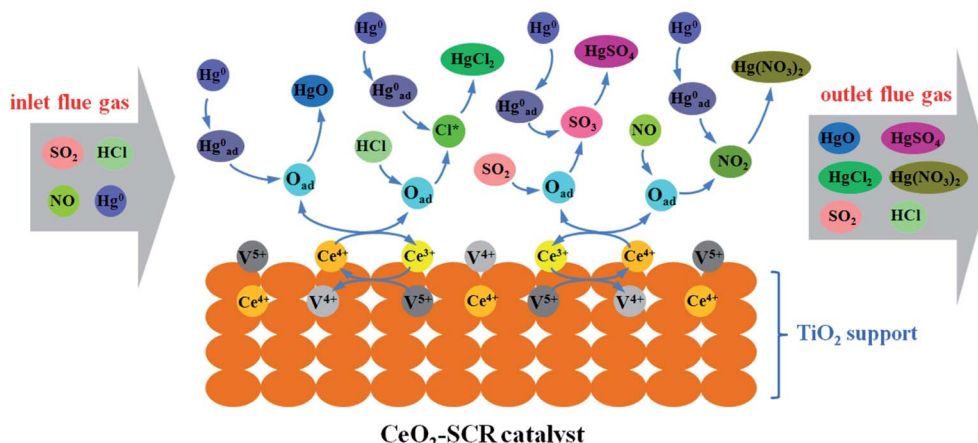


Fig. 13 Description of the mechanism of  $\text{CeO}_2$  modification on the synergistic  $\text{Hg}^0$  removal performance of commercial SCR catalyst.

with those for the fresh one. The results indicated that the intensity of both the  $\text{O}_{\text{ad}}$  and  $\text{V}^{5+}$  peaks reduced apparently after the reaction, as shown in Fig. 12(b) and (c). The variation could be observed more intuitively by the results in Table 4 that the ratios of  $\text{O}_{\text{ad}}$  and  $\text{V}^{5+}$  in the corresponding elements decreased from 32.5% to 27% and from 60.8% to 54.7%, respectively, in the reaction process, while the ratio of  $\text{Ce}^{3+}$  increased from 16.6% to 20.5%. The variation trends of the ratios of  $\text{O}_{\text{ad}}$  and  $\text{Ce}^{3+}$  on the catalyst were in accordance with those in the related literatures after the catalysts were spent.<sup>19,68</sup> The decline of the ratio of  $\text{O}_{\text{ad}}$  demonstrated it indeed participated in the catalytic reactions as the active substance. And the decrease of the proportion of  $\text{V}^{5+}$  suggested the redox behavior between element V and Ce on the catalyst during the reactions, which could be expressed by eqn (13). Combining the eqn (13) with the previous eqn (5), it could be seen that it occurred the process of the redox transformation between  $\text{Ce}^{3+}$  and  $\text{Ce}^{4+}$  on the surface, in which the chemisorbed oxygen was generated. The formed  $\text{O}_{\text{ad}}$  then involved in the catalytic reactions such as eqn (6), (7) and (9)–(12) so that the performance of the catalyst for synergistic  $\text{Hg}^0$  removal in SFG was improved. Besides  $\text{O}_{\text{ad}}$ , the ratio of  $\text{O}_{\text{hyd}}$  increased by 7.4% in the spent catalyst. On one hand,  $\text{H}_2\text{O}$  contained in the flue gas adsorbed on the catalyst and formed hydroxyl during the reaction, which caused the competitive adsorption with  $\text{Hg}^0$  and led to the inhibition of  $\text{H}_2\text{O}$  on  $\text{Hg}^0$  removal efficiency; on the other hand, the increased proportion of  $\text{O}_{\text{hyd}}$  might also be due to the generated  $\text{H}_2\text{O}$  of eqn (7), thereby further demonstrating the occurrence of this reaction.



Combining the experimental results and the XPS analysis conclusions, the modification effects of  $\text{CeO}_2$  on commercial SCR catalyst was mainly owed to the more sufficient chemisorbed oxygen which derived from the interaction between element V and Ce and the redox transformation between  $\text{Ce}^{3+}$  and  $\text{Ce}^{4+}$  on the catalyst surface. The abundant  $\text{O}_{\text{ad}}$  improved the catalytic activity of the catalyst and the promotion of related

flue gas components such as  $\text{HCl}$  on the  $\text{Hg}^0$  removal efficiency. Integrating these factors, the catalytic property for synergistic  $\text{Hg}^0$  removal was enhanced by the  $\text{CeO}_2$  modification. The modification process was described more vividly and specifically by the illustration shown in Fig. 13.

## 4. Conclusions

$\text{CeO}_2$  modified commercial SCR catalyst was prepared and investigated for NO and synergistic  $\text{Hg}^0$  removal. The research results indicated that the  $\text{CeO}_2$  loading improved a series of properties of the catalyst. Concretely, the BET surface area, the dispersity of the metal oxides on  $\text{TiO}_2$  support and the redox behavior were increased with the introduction of  $\text{CeO}_2$  into the catalyst, which was favorable to the catalytic activity. The catalyst with the  $\text{CeO}_2$  content of 4% exhibited the optimal performance for simultaneous NO and  $\text{Hg}^0$  removal. The NO conversion of 4%  $\text{CeO}_2$ -SCR was as high as 90.5% at 300 °C in SFG with excellent  $\text{N}_2$  selectivity, while the synergistic  $\text{Hg}^0$  removal efficiency could reach 78.2% under the same condition. Owing to the abundant chemisorbed oxygen generated from the synergy of  $\text{V}_2\text{O}_5$  and  $\text{CeO}_2$  and the redox transformation between  $\text{Ce}^{3+}$  and  $\text{Ce}^{4+}$ , the  $\text{Hg}^0$  removal activity, the  $\text{HCl}$  utilization and  $\text{NH}_3$ -resistance in  $\text{Hg}^0$  removal process and the promotion of  $\text{SO}_2$  and NO on  $\text{Hg}^0$  removal efficiency were improved over 4%  $\text{CeO}_2$ -SCR compared to over the raw catalyst. On account of these factors, the  $\text{CeO}_2$  modification made an enhancement on the synergistic  $\text{Hg}^0$  removal performance of the commercial SCR catalyst in simulated coal-fired flue gas, especially under low  $\text{HCl}$  concentration. Therefore, the  $\text{CeO}_2$  modified commercial SCR catalyst was a potential candidate to be practically applied in coal combustion power plant for NO and synergistic mercury removal.

## Conflicts of interest

There are no conflicts to declare.



## Acknowledgements

This research was supported by the Fundamental Research Fund of Shandong University (No. 2020GN008), the National Key Research and Development Program of China (No. 2016YFB0600604), the National Nature Science Foundation of China (NSFC) (No. 41672148) and the Foundation of State Key Laboratory of Coal Combustion (No. FSKLCCA1910). The authors would like to thank the Analysis and Test Center of Huazhong University of Science & Technology for the characterization work.

## References

- 1 P. J. Landrigan, R. O. Wright and L. S. Birnbaum, Mercury toxicity in children, *Science*, 2013, **342**, 1447.
- 2 UNEP, *Global mercury assessment 2018*, UNEP Chemicals and Health Branch, Geneva, Switzerland, 2019.
- 3 M. Rumayor, M. Díaz-Somoano, M. A. Lopez-Anton and M. R. Martínez-Tarazona, Application of thermal desorption for the identification of mercury species in solids derived from coal utilization, *Chemosphere*, 2015, **119**, 459–465.
- 4 Q. Wu, S. Wang, K. Liu, G. Li and J. Hao, Emission-limit-oriented strategy to control atmospheric mercury emissions in coal-fired power plants toward the implementation of the Minamata Convention, *Environ. Sci. Technol.*, 2008, **52**, 11087–11093.
- 5 Q. Shi, Y. Wang, X. Zhang, B. Shen, F. Wang and Y. Zhang, Hierarchically porous biochar synthesized with  $\text{CaCO}_3$  template for efficient  $\text{Hg}^0$  adsorption from flue gas, *Fuel Process. Technol.*, 2020, **199**, 106247.
- 6 X. Geng, Y. Duan, S. Zhao, Y. Xu, T. Huang, J. Hu and S. Ren, Study of mercury-removal performance of mechanical-chemical-brominated coal-fired fly ash, *Energy Fuels*, 2019, **33**, 6670–6677.
- 7 G. Busca, M. A. Larrubia, L. Arrighi and G. Ramis, Catalytic abatement of  $\text{NO}_x$ : chemical and mechanistic aspects, *Catal. Today*, 2005, **107–108**, 139–148.
- 8 P. G. Smirniotis, P. M. Sreekanth, D. A. Peña and R. G. Jenkins, Manganese oxide catalysts supported on  $\text{TiO}_2$ ,  $\text{Al}_2\text{O}_3$ , and  $\text{SiO}_2$ : a comparison for low-temperature SCR of NO with  $\text{NH}_3$ , *Ind. Eng. Chem. Res.*, 2006, **45**, 6436–6443.
- 9 C. Peng, J. Liang, H. Peng, R. Yan, W. Liu, Z. Wang, P. Wu and X. Wang, Design and synthesis of Cu/ZSM-5 catalyst via a facile one-pot dual-template strategy with controllable Cu content for removal of  $\text{NO}_x$ , *Ind. Eng. Chem. Res.*, 2018, **57**, 14967–14976.
- 10 S. Eswaran and H. G. Stenger, Understanding mercury conversion in selective catalytic reduction (SCR) catalysts, *Energy Fuels*, 2005, **19**, 2328–2334.
- 11 A. Suarez Negreira and J. Wilcox, Role of  $\text{WO}_3$  in the  $\text{Hg}^0$  oxidation across the  $\text{V}_2\text{O}_5\text{--WO}_3\text{--TiO}_2$  SCR catalyst: a DFT study, *J. Phys. Chem. C*, 2013, **117**, 24397–24406.
- 12 J. Yang, Q. Li, M. Li, W. Zhu, Z. Yang, W. Qu, Y. Hu and H. Li, In situ decoration of selenide on copper foam for the efficient immobilization of gaseous elemental mercury, *Environ. Sci. Technol.*, 2020, **54**, 2022–2030.
- 13 H. Kamata, S. Ueno, T. Naito, A. Yamaguchi and S. Ito, Mercury oxidation by hydrochloric acid over a  $\text{VO}_x\text{/TiO}_2$  catalyst, *Catal. Commun.*, 2008, **9**, 2441–2444.
- 14 C. L. Senior, Oxidation of mercury across selective catalytic reduction catalysts in coal-fired power plants, *J. Air Waste Manage. Assoc.*, 2006, **56**, 23–31.
- 15 W. Lee and G.-N. Bae, Removal of elemental mercury ( $\text{Hg}(0)$ ) by nanosized  $\text{V}_2\text{O}_5\text{/TiO}_2$  catalysts, *Environ. Sci. Technol.*, 2009, **43**, 1522–1527.
- 16 H. Kamata, S. Ueno, T. Naito and A. Yukimura, Mercury oxidation over the  $\text{V}_2\text{O}_5(\text{WO}_3)\text{/TiO}_2$  commercial SCR catalyst, *Ind. Eng. Chem. Res.*, 2008, **47**, 8136–8141.
- 17 H. Li, Y. Li, C.-Y. Wu and J. Zhang, Oxidation and capture of elemental mercury over  $\text{SiO}_2\text{--TiO}_2\text{--V}_2\text{O}_5$  catalysts in simulated low-rank coal combustion flue gas, *Chem. Eng. J.*, 2011, **169**, 186–193.
- 18 W. Gao, Q. Liu, C.-Y. Wu, H. Li, Y. Li, J. Yang and G. Wu, Kinetics of mercury oxidation in the presence of hydrochloric acid and oxygen over a commercial SCR catalyst, *Chem. Eng. J.*, 2013, **220**, 53–60.
- 19 L. Zhao, C. Li, J. Zhang, X. Zhang, F. Zhan, J. Ma, Y. Xie and G. Zeng, Promotional effect of  $\text{CeO}_2$  modified support on  $\text{V}_2\text{O}_5\text{--WO}_3\text{/TiO}_2$  catalyst for elemental mercury oxidation in simulated coal-fired flue gas, *Fuel*, 2015, **153**, 361–369.
- 20 Y. Cao, Z. Gao, J. Zhu, Q. Wang, Y. Huang, C. Chiu, B. Parker, P. Chu and W. Pan, Impacts of halogen additions on mercury oxidation, in a slipstream selective catalyst reduction (SCR) reactor when burning sub-bituminous coal, *Environ. Sci. Technol.*, 2008, **42**, 256–261.
- 21 C. W. Lee, R. K. Srivastava, S. B. Ghorishi, J. Karwowski, T. W. Hastings and J. C. Hirschi, Pilot-scale study of the effect of selective catalytic reduction catalyst on mercury speciation in illinois and powder river basin coal combustion flue gases, *J. Air Waste Manage. Assoc.*, 2006, **56**, 643–649.
- 22 X. Gao, Y. Jiang, Y. Zhong, Z. Luo and K. Cen, The activity and characterization of  $\text{CeO}_2\text{--TiO}_2$  catalysts prepared by the sol-gel method for selective catalytic reduction of NO with  $\text{NH}_3$ , *J. Hazard. Mater.*, 2010, **174**, 734–739.
- 23 H. Li, C.-Y. Wu, Y. Li and J. Zhang,  $\text{CeO}_2\text{--TiO}_2$  catalysts for catalytic oxidation of elemental mercury in low-rank coal combustion flue gas, *Environ. Sci. Technol.*, 2011, **45**, 7394–7400.
- 24 X. Fan, C. Li, G. Zeng, X. Zhang, S. Tao, P. Lu, Y. Tan and D. Luo,  $\text{Hg}^0$  removal from simulated flue gas over  $\text{CeO}_2\text{/HZSM-5}$ , *Energy Fuels*, 2012, **26**, 2082–2089.
- 25 Y. Wang, B. Shen, C. He, S. Yue and F. Wang, Simultaneous removal of NO and  $\text{Hg}^0$  from flue gas over  $\text{Mn-Ce/Ti-PILCs}$ , *Environ. Sci. Technol.*, 2015, **49**, 9355–9363.
- 26 L. Chen, J. Li and M. Ge, Promotional effect of Ce-doped  $\text{V}_2\text{O}_5\text{--WO}_3\text{/TiO}_2$  with low vanadium loadings for selective catalytic reduction of  $\text{NO}_x$  by  $\text{NH}_3$ , *J. Phys. Chem. C*, 2009, **113**, 21177–21184.
- 27 L. Song, J. Chao, Y. Fang, H. He, J. Li, W. Qiu and G. Zhang, Promotion of ceria for decomposition of ammonia bisulfate



over  $V_2O_5$ – $MoO_3$ /TiO<sub>2</sub> catalyst for selective catalytic reduction, *Chem. Eng. J.*, 2016, **303**, 275–281.

28 H. Li, J. Miao, Q. Su, Y. Yu, Y. Chen, J. Chen and J. Wang, Improvement in alkali metal resistance of commercial  $V_2O_5$ – $WO_3$ /TiO<sub>2</sub> SCR catalysts modified by Ce and Cu, *J. Mater. Sci.*, 2019, **54**, 14707–14719.

29 A. Zhang, W. Zheng, J. Song, S. Hu, Z. Liu and J. Xiang, Cobalt manganese oxides modified titania catalysts for oxidation of elemental mercury at low flue gas temperature, *Chem. Eng. J.*, 2014, **236**, 29–38.

30 W. Xu, H. Wang, X. Zhou and T. Zhu, CuO/TiO<sub>2</sub> catalysts for gas-phase Hg<sup>0</sup> catalytic oxidation, *Chem. Eng. J.*, 2014, **243**, 380–385.

31 C. Antuna-Nieto, E. Rodríguez, M. A. Lopez-Antón, R. García and M. R. Martínez-Tarazona, A candidate material for mercury control in energy production processes: carbon foams loaded with gold, *Energy*, 2018, **159**, 630–637.

32 S. Zhang, Y. Zhao, M. Díaz-Somoano, J. Yang and J. Zhang, Synergistic mercury removal over the CeMnO<sub>3</sub> perovskite structure oxide as a selective catalytic reduction catalyst from coal combustion flue gas, *Energy Fuels*, 2018, **32**, 11785–11795.

33 S. Zhang, Y. Zhao, Z. Wang, J. Zhang, L. Wang and C. Zheng, Integrated removal of NO and mercury from coal combustion flue gas using manganese oxides supported on TiO<sub>2</sub>, *J. Environ. Sci.*, 2017, **53**, 141–150.

34 S. Zhang, Y. Zhao, J. Yang, Y. Zhang, P. Sun, X. Yu, J. Zhang and C. Zheng, Simultaneous NO and mercury removal over MnO<sub>x</sub>/TiO<sub>2</sub> catalyst in different atmospheres, *Fuel Process. Technol.*, 2017, **166**, 282–290.

35 S. Zhang, Y. Zhao, J. Yang, J. Zhang and C. Zheng, Fe-modified MnO<sub>x</sub>/TiO<sub>2</sub> as the SCR catalyst for simultaneous removal of NO and mercury from coal combustion flue gas, *Chem. Eng. J.*, 2018, **348**, 618–629.

36 C. Orsenigo, L. Lietti, E. Tronconi, P. Forzatti and F. Bregani, Dynamic investigation of the role of the surface sulfates in NO<sub>x</sub> reduction and SO<sub>2</sub> oxidation over  $V_2O_5$ – $WO_3$ /TiO<sub>2</sub> catalysts, *Ind. Eng. Chem. Res.*, 1998, **37**, 2350–2359.

37 H. Xu, Y. Ma, S. Zhao, W. Huang, Z. Qu and N. Yan, Enhancement of Ce<sub>1-x</sub>Sn<sub>x</sub>O<sub>2</sub> support in LaMnO<sub>3</sub> for the catalytic oxidation and adsorption of elemental mercury, *RSC Adv.*, 2016, **6**, 63559–63567.

38 N. Yang, R. Guo, Y. Tian, W. Pan, Q. Chen, Q. Wang, C. Lu and S. Wang, The enhanced performance of ceria by HF treatment for selective catalytic reduction of NO with NH<sub>3</sub>, *Fuel*, 2016, **179**, 305–311.

39 P. Wang, Q. Wang, X. Ma, R. Guo and W. Pan, The influence of F and Cl on Mn/TiO<sub>2</sub> catalyst for selective catalytic reduction of NO with NH<sub>3</sub>: a comparative study, *Catal. Commun.*, 2015, **71**, 84–87.

40 X. Gao, Y. Jiang, Y. Fu, Y. Zhong, Z. Luo and K. Cen, Preparation and characterization of CeO<sub>2</sub>/TiO<sub>2</sub> catalysts for selective catalytic reduction of NO with NH<sub>3</sub>, *Catal. Commun.*, 2010, **11**, 465–469.

41 Z. Wu, B. Jiang, Y. Liu, W. Zhao and B. Guan, Experimental study on a low-temperature SCR catalyst based on MnO<sub>x</sub>/TiO<sub>2</sub> prepared by sol-gel method, *J. Hazard. Mater.*, 2007, **145**, 488–494.

42 H. Li, C.-Y. Wu, Y. Li and J. Zhang, Superior activity of MnO<sub>x</sub>–CeO<sub>2</sub>/TiO<sub>2</sub> catalyst for catalytic oxidation of elemental mercury at low flue gas temperatures, *Appl. Catal., B*, 2012, **111**–**112**, 381–388.

43 D. A. Peña, B. S. Uphade and P. G. Smirniotis, TiO<sub>2</sub>-supported metal oxide catalysts for low-temperature selective catalytic reduction of NO with NH<sub>3</sub>: I. Evaluation and characterization of first row transition metals, *J. Catal.*, 2004, **221**, 421–431.

44 L. Zhao, C. Li, S. Li, Y. Wang, J. Zhang, T. Wang and G. Zeng, Simultaneous removal of elemental mercury and NO in simulated flue gas over  $V_2O_5$ /ZrO<sub>2</sub>–CeO<sub>2</sub> catalyst, *Appl. Catal., B*, 2016, **198**, 420–430.

45 S. A. Benson, J. D. Laumb, C. R. Crocker and J. H. Pavlish, SCR catalyst performance in flue gases derived from subbituminous and lignite coals, *Fuel Process. Technol.*, 2005, **86**, 577–613.

46 J. Zhang, F. Liu, J. Liang, H. Yu, W. Liu, X. Wang, H. Peng and P. Wu, Exploring the nanosize effect of mordenite zeolites on their performance in the removal of NO<sub>x</sub>, *Ind. Eng. Chem. Res.*, 2019, **58**, 8625–8635.

47 Y. Li, P. D. Murphy, C.-Y. Wu, K. W. Powers and J.-C. J. Bonzongo, Development of silica/vanadia/titania catalysts for removal of elemental mercury from coal-combustion flue gas, *Environ. Sci. Technol.*, 2008, **42**, 5304–5309.

48 F. Scala and S. Cimino, Elemental mercury capture and oxidation by a regenerable manganese-based sorbent: the effect of gas composition, *Chem. Eng. J.*, 2015, **278**, 134–139.

49 S. Zhang, M. Díaz-Somoano, Y. Zhao, J. Yang and J. Zhang, Research on the mechanism of elemental mercury removal over Mn-based SCR catalysts by a developed Hg-TPD method, *Energy Fuels*, 2019, **33**, 2467–2476.

50 H. Li, L. Zhu, S. Wu, Y. Liu and K. Shih, Synergy of CuO and CeO<sub>2</sub> combination for mercury oxidation under low-temperature selective catalytic reduction atmosphere, *Int. J. Coal Geol.*, 2017, **170**, 69–76.

51 H. Li, C.-Y. Wu, Y. Li, L. Li, Y. Zhao and J. Zhang, Role of flue gas components in mercury oxidation over TiO<sub>2</sub> supported MnO<sub>x</sub>–CeO<sub>2</sub> mixed-oxide at low temperature, *J. Hazard. Mater.*, 2012, **243**, 117–123.

52 Y. Zhuang, J. Laumb, R. Liggett, M. Holmes and J. Pavlish, Impacts of acid gases on mercury oxidation across SCR catalyst, *Fuel Process. Technol.*, 2007, **88**, 929–934.

53 W. Xu, H. He and Y. Yu, Deactivation of a Ce/TiO<sub>2</sub> catalyst by SO<sub>2</sub> in the selective catalytic reduction of NO by NH<sub>3</sub>, *J. Phys. Chem. C*, 2009, **113**, 4426–4432.

54 S. Gao, P. Wang, F. Yu, H. Wang and Z. Wu, Dual resistance to alkali metals and SO<sub>2</sub>: vanadium and cerium supported on sulfated zirconia as an efficient catalyst for NH<sub>3</sub>-SCR, *Catal. Sci. Technol.*, 2016, **6**, 8148–8156.

55 H. Xu, Y. Ma, B. Mu, W. Huang, Q. Hong, Y. Liao, Z. Qu and N. Yan, Enhancing the catalytic oxidation of elemental mercury and suppressing sulfur-toxic adsorption sites from



SO<sub>2</sub>-containing gas in Mn-SnS<sub>2</sub>, *J. Hazard. Mater.*, 2020, **392**, 122230.

56 G. Busca, L. Lietti, G. Ramis and F. Berti, Chemical and mechanistic aspects of the selective catalytic reduction of NO<sub>x</sub> by ammonia over oxide catalysts: a review, *Appl. Catal., B*, 1998, **18**, 1–36.

57 P. Wang, S. Su, J. Xiang, H. You, F. Cao, L. Sun, S. Hu and Y. Zhang, Catalytic oxidation of Hg<sup>0</sup> by MnO<sub>x</sub>–CeO<sub>2</sub>/γ-Al<sub>2</sub>O<sub>3</sub> catalyst at low temperatures, *Chemosphere*, 2014, **101**, 49–54.

58 G. Qi, R. T. Yang and R. Chang, MnO<sub>x</sub>–CeO<sub>2</sub> mixed oxides prepared by co-precipitation for selective catalytic reduction of NO with NH<sub>3</sub> at low temperatures, *Appl. Catal., B*, 2004, **51**, 93–106.

59 J. Yang, Y. Zhao, J. Zhang and C. Zheng, Regenerable cobalt oxide loaded magnetosphere catalyst from fly ash for mercury removal in coal combustion flue gas, *Environ. Sci. Technol.*, 2014, **48**, 14837–14843.

60 Q. Wan, L. Duan, J. Li, L. Chen, K. He and J. Hao, Deactivation performance and mechanism of alkali (earth) metals on V<sub>2</sub>O<sub>5</sub>–WO<sub>3</sub>/TiO<sub>2</sub> catalyst for oxidation of gaseous elemental mercury in simulated coal-fired flue gas, *Catal. Today*, 2011, **175**, 189–195.

61 Y. Jiang, Z. Xing, X. Wang, S. Huang, X. Wang and Q. Liu, Activity and characterization of a Ce–W–Ti oxide catalyst prepared by a single step sol-gel method for selective catalytic reduction of NO with NH<sub>3</sub>, *Fuel*, 2015, **151**, 124–129.

62 W. Yao, Y. Liu, X. Wang, X. Weng, H. Wang and Z. Wu, The superior performance of sol-gel made Ce–O–P catalyst for selective catalytic reduction of NO with NH<sub>3</sub>, *J. Phys. Chem. C*, 2016, **120**, 221–229.

63 L. Li, L. Chen, M. Kong, Q. Liu and S. Ren, New insights into the deactivation mechanism of V<sub>2</sub>O<sub>5</sub>–WO<sub>3</sub>/TiO<sub>2</sub> catalyst during selective catalytic reduction of NO with NH<sub>3</sub>: synergies between arsenic and potassium species, *RSC Adv.*, 2019, **9**, 37724–37732.

64 S. He, J. Zhou, Y. Zhu, Z. Luo, M. Ni and K. Cen, Mercury oxidation over a vanadia-based selective catalytic reduction catalyst, *Energy Fuels*, 2009, **23**, 253–259.

65 Y. Li, W. Liu, R. Yan, J. Liang, T. Dong, Y. Mi, P. Wu, Z. Wang, H. Peng and T. An, Hierarchical three-dimensionally ordered macroporous Fe–V binary metal oxide catalyst for low temperature selective catalytic reduction of NO<sub>x</sub> from marine diesel engine exhaust, *Appl. Catal., B*, 2020, **268**, 118455.

66 R. Yan, S. Lin, Y. Li, W. Liu, Y. Mi, C. Tang, L. Wang, P. Wu and H. Peng, Novel shielding and synergy effects of Mn–Ce oxides confined in mesoporous zeolite for low temperature selective catalytic reduction of NO<sub>x</sub> with enhanced SO<sub>2</sub>/H<sub>2</sub>O tolerance, *J. Hazard. Mater.*, 2020, **396**, 122592.

67 R. Fan, Z. Li, Y. Wang, C. Zhang, Y. Wang, Z. Ding, X. Guo and R. Wang, Effects of WO<sub>3</sub> and SiO<sub>2</sub> doping on CeO<sub>2</sub>–TiO<sub>2</sub> catalysts for selective catalytic reduction of NO with ammonia, *RSC Adv.*, 2020, **10**, 5845–5852.

68 J. Yang, M. Zhang, H. Li, W. Qu, Y. Zhao and J. Zhang, Simultaneous NO reduction and Hg<sup>0</sup> oxidation over La<sub>0.8</sub>Ce<sub>0.2</sub>MnO<sub>3</sub> perovskite catalysts at low temperature, *Ind. Eng. Chem. Res.*, 2018, **57**, 9374–9385.

